Calendar Time Local Earthquake Forecasts from Earthquake Nowcasts: A Do-It-Yourself (DIY) Ensemble Method

John B Rundle[1,2,3], Ian Baughman[1], Andrea Donnellan[4,3], Lisa Grant[5], Geoffrey Fox[6], Kazuyoshi Nanjo[7]

[1] University of California, Davis, CA
[2] Santa Fe Institute, Santa Fe, NM
[3] Jet Propulsion Laboratory, Pasadena, CA
[4] Purdue University, West Lafayette, IN
[5] University of California, Irvine, CA
[6] University of Virginia, Charlottesville, VA
[7]Shizuoka University, Japan

Abstract

A previous paper (JBR et al., 2025) discussed a method that builds on local earthquake nowcasts to produce fixed natural time forecasts, where natural time represents counts of small earthquakes since the last large earthquake. In this second paper we extend the natural time forecast to calendar time forecasts using an ensemble approach. The Gutenberg-Richter (GR) magnitude-frequency relation, which was the basis for both methods, states that for every large target earthquake of magnitude greater than M_T , there are on average N_{GR} small earthquakes of magnitude M_S. The only assumption in our method is that the statistics of the local region are the same as in the larger surrounding regions. The method has significant skill, as defined by the Receiver Operating Characteristic (ROC) test, which improves as time since the last major earthquake increases. The probability is conditioned on the number of small earthquakes $n(t)$ that have occurred since the last large earthquake. We do not need to assume a probability model, the probability is instead computed directly as the Positive Predictive Value (PPV) associated with the ROC curve. We find that for short time intervals (months), the forecast shows strong main shock clustering, followed by a gradual buildup of probability over the following years leading to the next large earthquake ("elastic rebound"). We apply the method to the same local region as in our first paper around Los Angeles, California, following the January 17, 1994 magnitude M6.7 Northridge earthquake.

Key Points

- Earthquake nowcasting uses counts of small earthquakes to determine the current real time risk of a large earthquake
- The technique can be used as a basis for earthquake forecasting in calendar time
- A major advantage is that the forecast probability curve is determined directly from the data itself, rather than being assumed

Plain Language Summary

Earthquake nowcasting is a recently developed method that allows the current progress of a seismically active region through its cycle of large damaging earthquakes to be determined. Forecasting and predicting the location and time of major earthquakes are long-sought goals. Unlike weather forecasting, the data needed for detailed and precise earthquake forecasting will always be incomplete. What can be observed is data represented by earthquake catalogs, which include the time, location, and magnitude of the events. In past works, we have shown that the current state of the local regions can be observed by counting the number of small earthquakes since the last large earthquake in a region. We have called this method earthquake nowcasting. In a very recent paper, we developed a new technique for extending earthquake nowcasts to earthquake forecasts in the "natural time" domain, where by natural time we mean counts of successive small earthquakes. In the present paper, we extend the method to the calendar time domain, thus answering the question, " what is the probability of a large earthquake of magnitude X in a small region during the next Y months?" We then illustrate these procedures by application to the region around Los Angeles, CA following the January 17, 1994 magnitude M6.7 Northridge earthquake. Major advantages of the proposed method are its basic simplicity, and the fact that there are no unknown parameters that must be assumed or set by arbitrary means.

Introduction

This is the second of a two-part series of papers introducing methods for computing local earthquake forecasts of future large earthquakes from local earthquake nowcasts. The first paper (Rundle et al., 2025) detailed a method to compute local forecasts for a fixed future natural time interval, where natural time is the count of small earthquakes since the last large earthquake. The current paper introduces a method to compute forecasts using a fixed future calendar time interval, using a regional ensemble method.

Previous papers have developed several techniques for earthquake nowcasting, which is based on using counts of small earthquakes to track the progression of the fault system through its cycle of large earthquake activity. The term nowcasting is used in the same sense as for weather and economic nowcasting (e.g., Rundle et al., 2016; Rundle et al., 2021a), the determination of the current state of a system in the recent past, current time, and the near future. Methods to produce earthquake nowcasts have been the subject of previous papers, a selection of which are: (Rundle et al., 2016; 2018; 2019a; 2019b; 2020; 2021a,b; 2022a,b; 2024; Pasari and Mehta, 2018; Pasari, 2019; Pasari, 2020; Pasari and Sharma, 2020; Chouliaras, 2009; Chouliaras et al., 2023; Perez-Oregon, 2020).

The most recent paper (Rundle et al., 2025) develops a technique to compute the probability of a future large earthquake directly from the catalog data, by the use of the Receiver Operating Characteristic (ROC). The ROC method, developed in the 1940's by the British with the advent of radar, considers all possible cases of a signal followed by an event:

- True positive (TP), where a signal is observed, followed by an event
- True negative (TN) where no signal is observed and no event follows

- False positive (FP), where a signal is observed and no event follows
- False negative (FN), where no signal is observed but an event follows

These are the basic quantities that we use in building the forecast.

The nowcasting method is applied to a small circle of arbitrary radius surrounding a point of interest, typically a city. Computing the probability then involves a training phase using an expanding series of larger rectangular regions surrounding the circle. These regions then comprise the training ensemble for the method. More specifically, training involves computation of the ROC curve, a plot of the True Positive Rate (TPR) vs. the False Positive Rate (FPR), where these are defined as e.g., (Mandrekar, 2010; Powers, 2011):

$$TPR = TP/(TP + FN) \quad (1)$$

$$FPR = FP/(FP + TN)$$

Once the ROC curve is computed for a member of the ensemble, the Positive Predictive Value (PPV) is then computed:

$$PPV = TP/(TP + FP) \quad (2)$$

The basic assumption in this method is that the catalog statistics of the surrounding region are the same as the statistics of the circular region. Or more specifically, we make what amounts to an ergodic assumption, that time averages can be replaced by space (or ensemble) averages.

This process produces a family of ROC and PPV curves, one corresponding to each member of the ensemble. Once we are in possession of these curves, we compute the mean curve and its standard deviation. Note that the area under the ROC curve (AUROC, or "skill") can be interpreted as the ability of a model to discriminate between, or to correctly classify, different categories of events. In our case, an event is the occurrence of a major earthquake vs. non-occurrence (Mandrekar, 2010; Powers, 2011).

Ensemble Construction

In Rundle et al. (2025), we used a fixed number of hypothesized future small earthquakes for our forecast interval. Counts of small earthquakes are an example of "natural time", the time scale that is relevant to the physics of the system. But these small earthquakes occur with unknown future frequency and timing. So a fixed future count is not as informative as it could be. Since human beings operate on calendar time, forecasts are most useful if a fixed future time interval is used.

This problem motivates the use of the ensemble approach. To implement this approach, we first define the minimum rectangular ensemble surround the circle of interest. We characterize this size as a rectangle with half width of size D_M. The criterion we use for the minimum rectangle size is to require a minimum of 20 large earthquakes of a target magnitude M_T. "Small earthquakes" are defined as events having magnitude $M_S < M_T$.

Additional members of the expanding ensemble are then considered as those with an increasing half width of value ΔD. For the example we show below, we find that $D_M = 3.1^o$. We then define an additional 29 members of the ensemble as those with $D = 3.3^o$, 3.4^o, 3.5^o, etc. thus $\Delta D = 0.1^o$, for a total number of ensemble members = 30.

For each member of the ensemble, we then classify "cycles of activity" between large events whose beginnings and endings are bounded by earthquakes of the target magnitude M_T. So an ensemble member with N_{ENS} large earthquakes will have N_{ENS} -1 cycles by this definition. These cycles of activity represent the training set for the simple machine learning application. Cycle j within ensemble member i ($C_{i,j}$) will have $n_{i,j}$ small earthquakes by definition.

A critically important point is to note that these increasingly large rectangular regions contain many more small earthquakes over the same time period than does the small circular region in which we wish to make the forecast. So in terms of "calendar time", "natural time" will pass increasingly more quickly in the successively larger ensemble members than it does in the small circular region.

Or to state the idea in another way, the rate of occurrence of events in a larger region R_L is higher than the rate in the circle R_C, $R_L > R_C$, so the natural time "clock" is running faster in the larger region than in the circle. This represents a kind of "special relativity of time", in analogy to special relativity in physics. As a result we need to apply a correction for this effect.

In Rundle et al. (2025), we used a single optimized large region surrounding the circle. We then applied a correction to the calendar time rate in the large region to match the rate in the circle. In the present application in which we use an ensemble of large regions, we are using a future forecast time interval T_F rather than a forecast number. So rather than scale the regions in time, we choose to scale the forecast time to a value appropriate for each large region in the ensemble:

$$T_{F,L} = (R_C / R_L) T_{F,C} \tag{3}$$

Here $T_{F,C}$ is the chosen forecast time of interest in the circle, and $T_{F,L}$ is the corresponding scaled forecast time in the region. Clearly, $T_{F,C} > T_{F,L}$ since $R_L > R_C$. As a result, each region in the ensemble will have a different scaled forecast time, the scaled forecast time decreasing as the linear dimension of the region increases.

Building the ROC Curve

To calculate the forecast probability for a fixed future time interval $T_{F,C}$ in the circle of interest, we build the ROC curve, which takes proper account of all 4 possibilities, TP, FP, TN, FN. From the ROC curve we can then compute the forecast probability, the positive predictive value PPV.

To build an ROC curve, we consider a sequence of small earthquakes in the circle following the last large earthquake. These small earthquakes in the circle catalog occur at a sequence of times that we denote by t_n, where $n_C = 1,...,N_C$. Similarly, in cycle j of ensemble i, denoted by $C_{i,j}$, there is some distinct number of small earthquakes $N_{i,j}$.

In a given cycle, there may be almost no small earthquakes where mainshocks cluster strongly in calendar time. In other cycles, there may be many small earthquakes where there is a comparatively large separation between mainshocks in calendar time.

Now consider a cycle $C_{i,j}$ having a total number $N_{i,j}$ of small earthquakes. As in Rundle et al. (2025), we define a nowcast value Φ by:

$$\Phi(n) = 1 - e^{-(n/N_{scale}))} \quad (4)$$

where N_{scale} is computed from the Gutenberg-Richter relation (e.g., Boore, 1989):

$$N_{scale} = e^{b(M_T - M_S)} \quad (5)$$

Here b is the Gutenberg-Richter b-value for the ensemble member. Equations (4)-(5) are equivalent to the Earthquake Potential State (EPS) as defined in (Rundle et al., (2016; 2018; 2019a; 2019b; 2020; 2021a,b; 2022; 2024).

These equations arise from the idea that the interval statistics of earthquakes are generally Poisson distributed (e.g., Gardner and Knopoff, 1974). Applying equations (4) and (5), we show a typical example of a nowcast timeseries in Figure 1 for a region surrounding Los Angeles, CA, which plots nowcast values as a function of time.

Using (4), all times in the ensemble of cycles are assigned nowcast values $\Phi([n_{i,j}])$ where $[n_{i,j}]$ is the set of sequence indices of the small earthquakes in the j^{th} cycle of the i^{th} ensemble member. As an explicit example, if there are 5 small earthquakes in cycle 3 of ensemble member 2, $[n_{2,3}] \in [1,2,3,4,5]$. Then $\Phi([n_{2,3}])$ would be a set of 5 values computed by applying equations (4) and (5) to the set $[n_{2,3}]$, yielding the set $[\Phi_1, \Phi_2, \Phi_3, \Phi_4, \Phi_5]$. Note that each of the events in $C_{i,j}$ has a time value as well as a sequence number, $t \in [t_1, t_2, t_3, t_4, t_5]$.

So the critical point is that each small event in the ensemble can be characterized by a nowcast value, a sequence index, and a time value. To build the ROC diagram, we adopt a set of threshold values, as has been explained in, e.g, Rundle et al. (2021a,b; 2022a,b; 2024) . For each ensemble member, we classify all points on the nowcast timeseries.

We start by selecting an arbitrary threshold value τ. Given a small event occurring at time t, we ask if that event's nowcast value is above or below the threshold. We also ask if the next target earthquake M_T occurs after time t but within the time interval $t + T_{F,L}$, where again, $T_{F,L}$ is the scaled forecast time for that ensemble member. Classification is then given by:

- TP, if the nowcast value is above the threshold τ, and the next target earthquake occurs within $t + T_{F,L}$ TP
- FP, if the nowcast value is above the threshold τ, and no earthquake occurs within interval $t + T_{F,L}$
- FN, if the nowcast value is below the threshold τ, and the next target earthquake occurs within interval $t + T_{F,L}$
- TN, if the nowcast value is below the threshold τ, and no target earthquake occurs within interval $t + T_{F,L}$

It should be noted that the ROC diagram is conditioned on the current number of events in the circle. For example, if the current number of small earthquakes in the circle is, for example 100, then no cycles of length less than 100 are used in the classification. Examples of conditional ROC diagrams will be shown below.

We should also explicitly note that the various computed quantities TP, TN, FP, FN are functions only of the threshold values, τ, so that we have TP(τ), TN(τ), FP(τ), FN(τ).

Computing the PPV Probability

To compute the PPV values (probabilities) at the times of the small events following the last large event in the circle, we use as threshold values τ the nowcast values for these small events defined by (4) and (5). So if there are 100 small earthquakes within the circle since the last large earthquake, we compute 100 values for $\Phi(n)$ and use these as our threshold set $[\tau(n)] \equiv [\Phi(n)]$.

Each of these small earthquakes then has a defined nowcast value, a sequence number, and an occurrence time, all of which are associated with the event. Again, note that the TP, FP, TN, FN are functions of the threshold only, which in this special case is the event nowcast value. Since the nowcast value is also a threshold, this association allows to identify specific event sequence numbers and event times with a PPV value.

Continuing the example in the previous section, we would then have a set of defined thresholds $[\tau] = [\Phi_1, \Phi_2, \Phi_3, \Phi_4, \Phi_5]$ with associated times $t \in [t_1, t_2, t_3, t_4, t_5]$. This allows us to associate the threshold values, which the TP, FP, TN, FN depend on, with event occurrence times in the circle.

Results and Discussion

We apply our method to a circular region of radius 125 km surrounding Los Angeles, CA, using a target magnitude M_T = 6 and small earthquake M_S = 3.49. The most recent large earthquake in the circle was the Northridge earthquake, having magnitude M=6.7, occurring on January 17, 1994.

The choice of circle radius is of course arbitrary, but we use a rule of thumb that the radius should be a 3-4 times the linear dimension of the aftershock zone of the previous large earthquake in the circle (see Figure 1). In addition, Chouliaras et al. (2023) have conducted a more quantitative analysis of appropriate circle radius for similar earthquake magnitudes in Greece, and also arrived at a radius of 125 km.

An additional criterion for the choice of radius is the "radius of significant ground shaking" for a given magnitude, for example the distance at which one might experience Mercalli Intensity VI (PGA ~ 0.1g) shaking. As Manyele and Mwambela (2014), Minson et al. (2021), and many others have shown, this distance is about 100-150 km for an M_T = 6 earthquake which is our minimum size for the forecast.

In Figure 2, we show a plot of 4 conditional ROC diagrams for a 1-year forecast assuming 1) no events have yet occurred in the circle; 2) 100 events have occurred in the circle; 3) 250 events have occurred in the circle; and 4) 447 events have occurred, the current number as of this writing. Notice that the area under the curve, or skill, increases later in the cycle.

The skill represents the ability of a forecast to discriminate among different cases: 1) future event occurring, or 2) no future event occurring. It can be seen that there is essentially no skill if the current number of circle events is small, but that the skill increases as more small events occur. Also note that the ROC diagrams in Figure 2 were constructed using a set of thresholds defined at 100 equidistant values between [0,1] (or [0, 100%]).

Also, for the purposes of these plots, we have used an ensemble of 30 regions, from 3.6° to 9.4° linear half-length as shown in the figures. The red curve represents the mean value

of the ROC for the ensemble, and the dashed lines represent the standard deviations. The cyan curves are the ROC values for the various members of the ensemble.

Figure 3 shows PPV plots for 1 year and 5 years for events in the circle. For these plots, we set the threshold $[\tau] = [\Phi_{\text{Circle}}]$, where Φ_{Circle} represents the nowcast values computed for the specific events and times in the circle. Again, the red curve represents the mean, the dashed curves are the standard deviations, and the cyan curves are the PPV curves for the various ensemble members.

The figures at top are for a forecast time of 1 year, and the figures on the bottom are for a forecast time of 5 years. The figures on the left use an ensemble of 30 regions, and the plots on the right use an ensemble of 60 regions. These figures show that the mean PPC curve is relatively insensitive to the number of regions in the ensemble.

It can be seen in Figure 3 that for the shorter forecast intervals, mainshock clustering dominates, i.e., initial high PPV values immediately following the last (Northridge) mainshock. In the following years, the PPV values gradually increase as the buildup to the next large earthquake occurs. For the longer forecast times, the mainshock clustering effect is increasingly less important.

In Figure 4 we show the final slide a movie that can be produce with the python code referenced below. The left side is the nowcast plot. At middle left is a "thermometer" whose value is the same as the current nowcast value. At middle right is the 5 year PPV plot, same as in Figure 3. At right is the plot of 447 small earthquakes that have occurred since the 1/17/1994 Northridge earthquake.

Acknowledgements. Research by JBR was supported in part by a grant from the Southern California Earthquake Center grant #SCON-00007927 to UC Davis, and by the John LaBrecque fund, a generous gift from John LaBrecque to the University of California, Davis. SCEC contribution number 15007**.** The authors would also like to acknowledge an informative conversation with Jeanne Hardebeck of the USGS.

Data. Data for this paper was downloaded from the USGS earthquake catalog for California, and are freely available there. An included method in the Python code mentioned above can be used to download these data for analysis.

References

Boore, D.M., 1989. The Richter scale: its development and use for determining earthquake source parameters. Tectonophysics, 166(1-3), pp.1-14.

Chouliaras, G, Seismicity anomalies prior to 8 June 2008, Mw=6.4 earthquake in Western Greece, *Nat. Hazards Earth Syst. Sci*., 9, 327–335 (2009)

Chouliaras, G., Skordas, E.S. and Sarlis, N.V., 2023. Earthquake nowcasting: Retrospective testing in Greece. *Entropy*, *25*(2), p.379.

Gardner, J. K., and Leon Knopoff, Is the sequence of earthquakes in Southern California, with aftershocks removed, Poissonian?, *Bulletin of the seismological society of America* 64.5, 1363-1367. (1974)

Holliday, JR, Rundle, JB, Turcotte, DL, Klein, W. and Tiampo, KF, Space-time correlation and clustering of major earthquakes, *Phys. Rev. Lett*., 97, 238501 (2006b)

Mandrekar, J.N., 2010. Receiver operating characteristic curve in diagnostic test assessment. Journal of thoracic oncology, 5(9), pp.1315-1316.

Manyele, A. and Mwambela, A., 2014. Simulated PGA Shaking Maps for the Magnitude 6.8 Lake Tanganyika earthquake of December 5, 2005 and the observed damages across South Western Tanzania. *IJSRP*, *4*, pp.1-5.

Minson, S.E., Baltay, A.S., Cochran, E.S., McBride, S.K. and Milner, K.R., 2021. Shaking is almost always a surprise: The earthquakes that produce significant ground motion. *Seismological Society of America*, *92*(1), pp.460-468.

Pasari, S. Nowcasting earthquakes in the Bay-of-Bengal region. *Pure Appl. Geophys.* 23, 537-559 (2019).

Pasari, S. Stochastic Modeling of Earthquake Interevent Counts (Natural Times) in Northwest Himalaya and Adjoining Regions. In: Bhattacharyya, S., Kumar, J. and Ghoshal, K. Mathematical Modeling and Computational Tools, *Springer Proceedings in Mathematics & Statistics*, 320, 495-501, Springer, Singapore (2020).

Pasari, S., and Mehta, A. 2018. Nowcasting earthquakes in the northwest Himalaya and surrounding regions. *Int. Arch. Photogramm. Remote Sens. Spatial Inf. Sci.*, XLII-5, 855–859 (2018).

Pasari, S. and Sharma, Y., 2020. Contemporary earthquake hazards in the West-northwest Himalaya: A statistical perspective through natural times. Seismological Society of America, 91(6), pp.3358-3369.

Perez-Oregon, Jennifer, Fernando Angulo-Brown, and Nicholas Vassiliou Sarlis. Nowcasting Avalanches as Earthquakes and the Predictability of Strong Avalanches in the Olami-Feder-Christensen Model. Entropy 22.11 (2020): 1228. (2020).

Powers, David M.W. Evaluation: From Precision, Recall and F-Measure to ROC, Informedness, Markedness & Correlation, Journal of Machine Learning Technologies. 2 (1): 37–63 (2011)

Rundle, J.B., Donnellan, A., Grant Ludwig, L, Gong, G., Turcotte, D.L. and Luginbuhl, M. Nowcasting earthquakes. *Earth and Space Science*, 3, 480-486 (2016).

Rundle, J.B., Luginbuhl, M., Giguere, A., and Turcotte, D.L. Natural time, nowcasting and the physics of earthquakes: Estimation of risk to global megacities. *Pure Appl. Geophys*., 175, 647-660 (2018).

Rundle, J.B., Luginbuhl, M., Khapikova, P. et al. Nowcasting Great Global Earthquake and Tsunami Sources, Pure Appl. Geophys. doi:10.1007/s00024-018-2039-y (2019a)

Rundle, JB, Giguere, A, Turcotte, DL, Crutchfield, JP, and Donnellan, A, Global seismic nowcasting with Shannon information entropy, Earth and Space Science, 6, 456-472 (2019b)

Rundle, J. B., and Andrea Donnellan, Nowcasting earthquakes in Southern California with machine learning: Bursts, swarms, and aftershocks may be related to levels of regional tectonic stress, *Earth and Space Science* 7.9 (2020): e2020EA0010

Rundle, J.B., Stein, S., Donnellan, A., Turcotte, D.L. Klein, W., and Saylor, C., The complex dynamics of earthquake fault systems: New approaches to forecasting and nowcasting of earthquakes, *Reports on Progress in Physics*, 84, 7, 076801, (2021a)

Rundle, J.B., Donnellan, A., Fox, GCF, Crutchfield, JP, and Granat, R., Nowcasting earthquakes: Imaging the earthquake cycle in California with machine learning, submitted to *Earth and Space Science*, (2021b).

Rundle, J.B., Yazbeck, J., Donnellan, A., Fox, G., Ludwig, L.G., Heflin, M. and Crutchfield, J. Optimizing earthquake nowcasting with machine learning: The role of strain hardening in the earthquake cycle. *Earth and Space Science*, *9*(11), p.e2022EA002343. (2022a)

Rundle, J.B., Donnellan, A., Fox, G. and Crutchfield, J.P., Nowcasting earthquakes by visualizing the earthquake cycle with machine learning: A comparison of two methods. Surveys in Geophysics, 43(2), pp.483-501 (2022b).

Rundle, J.B., Baughman, I. and Zhang, T. Nowcasting earthquakes with stochastic simulations: Information entropy of earthquake catalogs. *Earth and Space Science*, *11*(6), p.e2023EA003367 (2024)

Rundle, JB, Baughman, I., Donnellan, A., Gran Ludwig, L, and Fox, GC, From local earthquake nowcasting to natural time forecasting: A simple Do-It-Yourself (DIY) method, *Earth and Space Science*, in press (2025).

Varotsos, P., Sarlis, N.V. and Skordas, E.S. Spatiotemporal complexity aspects on the interrelation between Seismic Electric Signals and seismicity, *Practica of Athens Academy*, 76, 294-321 (2001).

Varotsos, P., Sarlis, N.V. and Skordas, E.S. *Natural Time Analysis: The new view of time. Precursory Seismic Electric Signals, Earthquakes and other Complex Time-Series.* Springer-Verlag, Berlin Heidelberg (2011).

Varotsos, P., Sarlis, N.V. and Skordas, E.S. Study of the temporal correlations in the magnitude time series before major earthquakes in Japan. *J. Geophys. Res. Space Phys.*, 119, 9192-9206 (2014).

Figure 1. Left: A typical example plot of the seismicity in the 10^o x 10^o region centered on Los Angeles from 1980-present. Red circles are the $M \geq 6$ earthquakes, small dots are the earthquakes having $M \geq 3.5$. Blue ellipse is a circle of radius 125 km. Right: A plot of the time series from 1980-present of the associated nowcast values computed from equations (4)-(5) in the text. Vertical dashed lines on the plot mark the boundaries of the earthquake cycles, blue for $M \geq 6$, red for $M \geq 7$. A typical earthquake cycle is shown by the double red arrows.

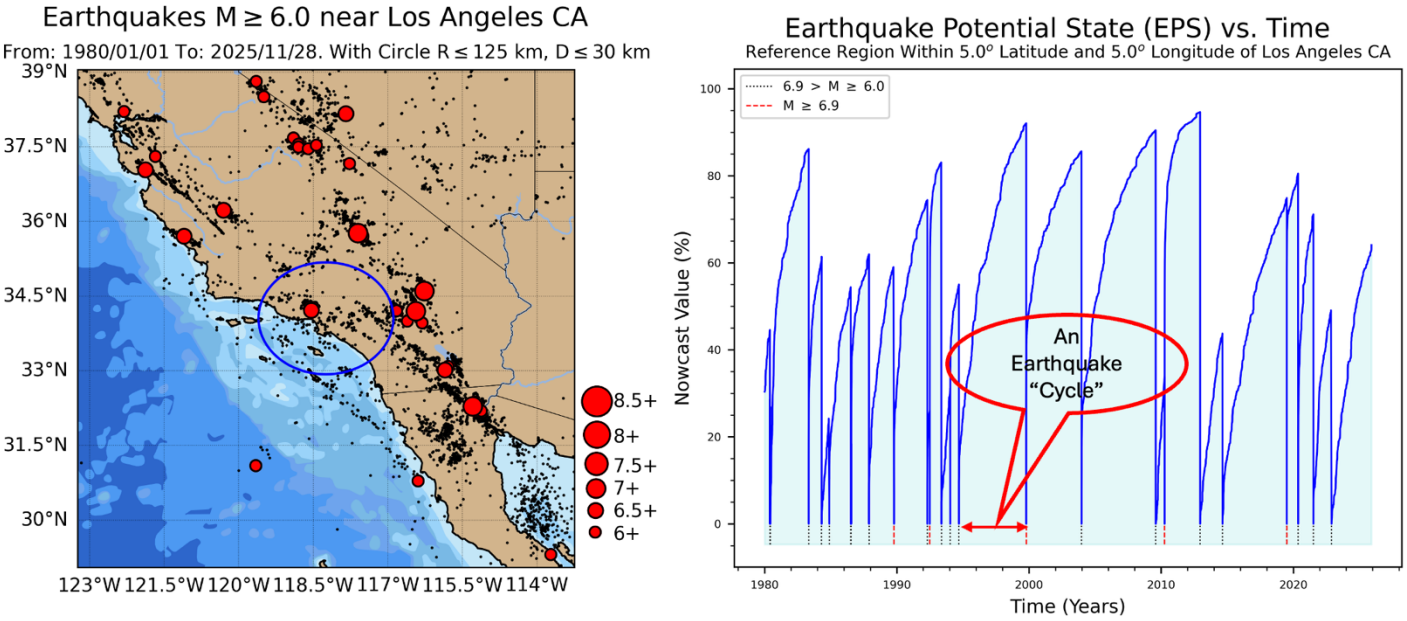

Figure 2. Conditional Receiver Operating Characteristic (ROC) diagrams for an ensemble of 30 regions from 3.6o to 6.5o surrounding Los Angeles, CA, at 0.1° interval half-widths, with a forecast time of T_F = 5 years. a) ROC diagram computed after no small earthquakes have occurred. b) ROC diagram computed after 150 small earthquakes have occurred. c) ROC diagram computed after 300 small earthquakes have occurred. d) ROC diagram computed after 447 small earthquakes have occurred, which is the number in the circle to date. The diagrams are conditional because only cycles with more events than the designated number (0, 150, 300, 447) of events are used to compute the ROC curves. Cyan curves are for the various ensemble members. Red curve is the mean value, dashed curves are the 1 standard deviation curves. Diagonal line is the no skill line. Skill for the curves are, respectively, 0.47, 0.78, 0.86, 0.90, showing that skill improves later in the earthquake cycle.

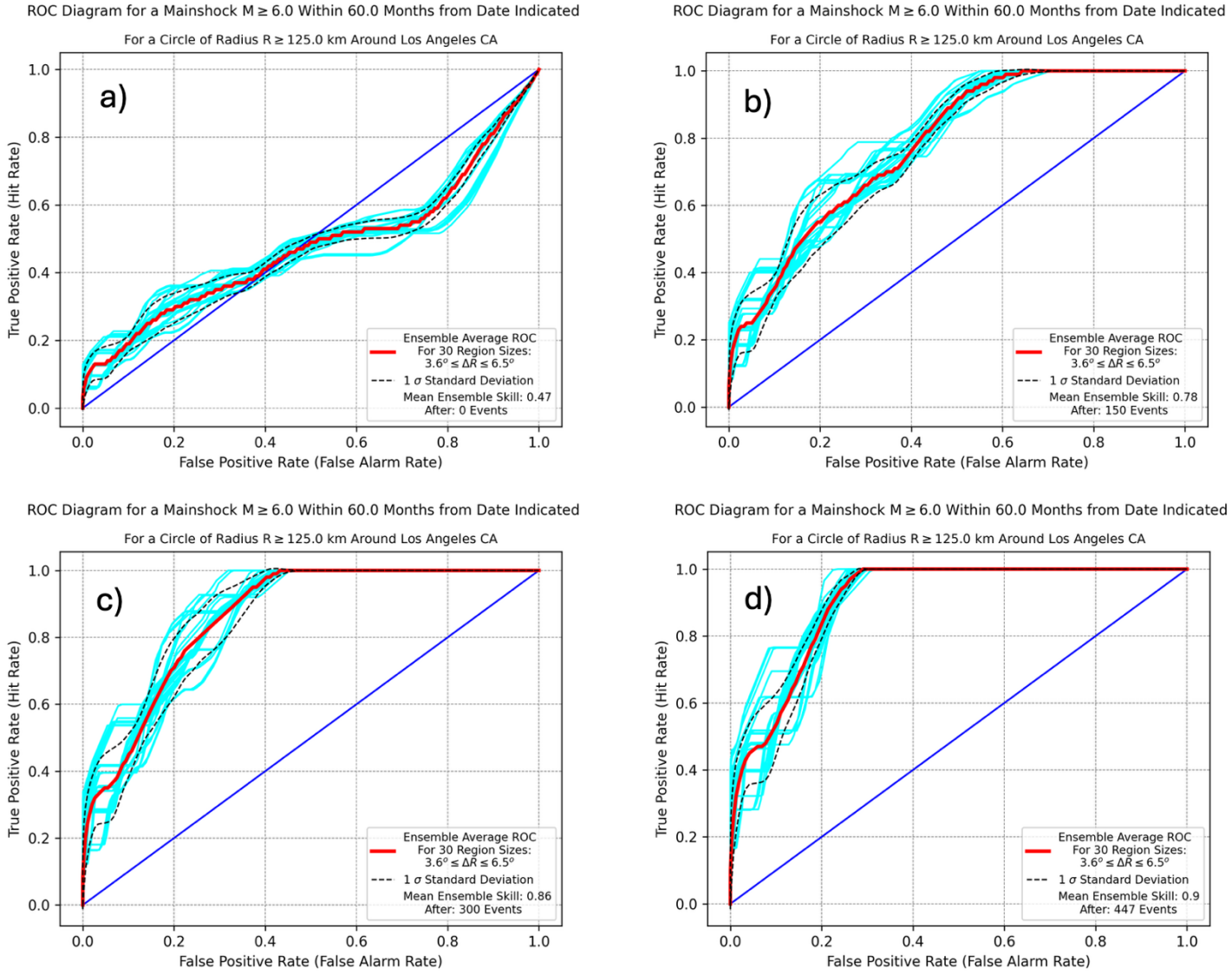

Figure 3. Plots of PPV, the probability of a future $M \geq 6$ earthquake, as function of time since the M6.7 Northridge, CA earthquake on 1/17/1994. a) Ensemble size = 30, Forecast time interval T_F = 1 year. b) Ensemble size = 60, Forecast time interval T_F = 1 year. c) Ensemble size = 30, Forecast time interval T_F = 5 years. d) Ensemble size = 60, Forecast time interval T_F = 5 years. Cyan-colored curves are for the various ensemble members. Red curve is the mean ensemble probability, and dashed curves are the 1-standard deviation curves. In figures a) and c), probability immediately after the mainshock is high, indicating a tendency for mainshock clustering. In figures b) and d) tectonic reloading over time following the Northridge earthquake is the primary process that can be seen.

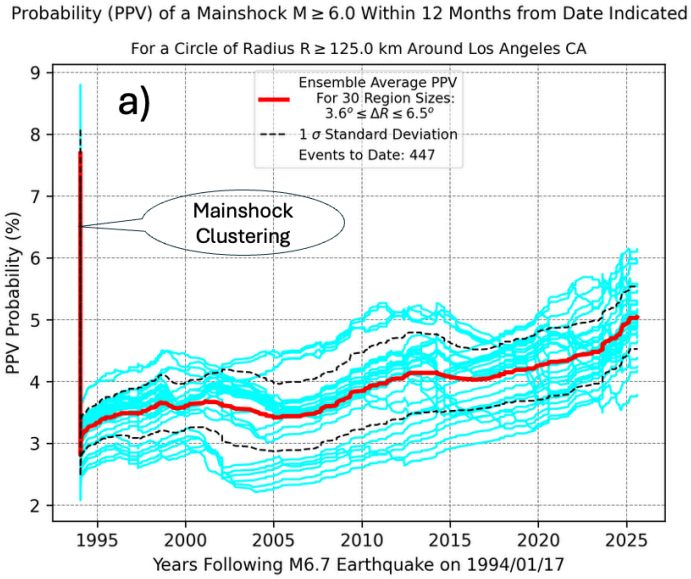

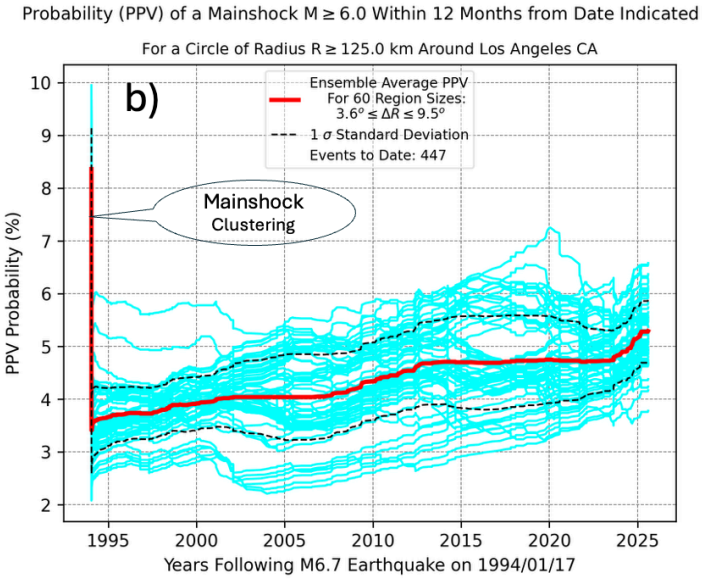

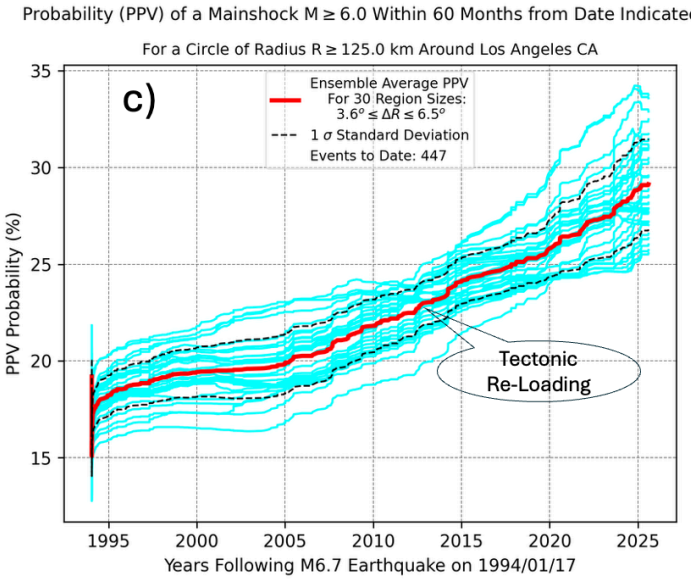

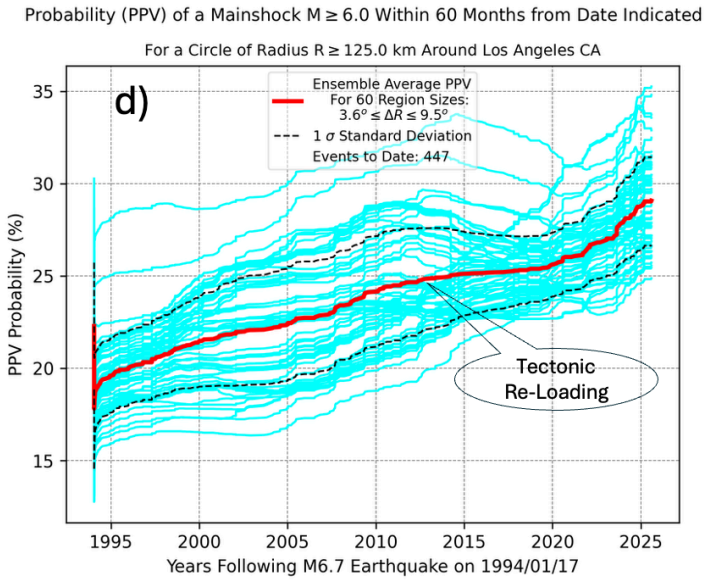

Figure 4. Final slide of a movie that can be produced with the python code, showing the current state of the target earthquake potential in the circle. a) Green bars represent the histogram of small earthquakes in the 45 complete earthquake cycles in the large region since 1970. The Cumulative Distribution Function (CDF) is derived from the histogram. The magenta curves close to the red curve represent the 1σ deviation from the histogram, again using a bootstrap method. The dashed blue line is the accumulation function, computed from equation (2). b) The red "thermometer" has the same value as the CDF (for easy reference), representing the EPS value. c) PPV vs. Time curve, the same as in Figure 3a. d) Total of small earthquakes following the 1994 Northridge earthquake up to the present time, 12/3/2025, color coded with more recent earthquakes in hotter colors. Large circle marks the epicenter of the Northridge mainshock. The current ensemble average probability for a future earthquake $M \geq 6$ is 29.1 ± 2.3% for a 5-Year PPV forecast. This value represents the Final Reckoning.